Soluble Aggregates in Aqueous Solutions of Polyion–Surfactant Ion Complex Salts and a Nonionic Surfactant

ARTICLE *in* THE JOURNAL OF PHYSICAL CHEMISTRY B · JUNE 2014

Impact Factor: 3.3 · DOI: 10.1021/jp411701g · Source: PubMed

6 AUTHORS, INCLUDING:

Matija Tomsic
University of Ljubljana
40 PUBLICATIONS **521** CITATIONS
SEE PROFILE

Dan Lundberg
CR Competence AB, Lund
30 PUBLICATIONS **318** CITATIONS
SEE PROFILE

Karin Schillén
Lund University
80 PUBLICATIONS **2,867** CITATIONS
SEE PROFILE

THE JOURNAL OF PHYSICAL CHEMISTRY B

Article

pubs.acs.org/JPCB

Soluble Aggregates in Aqueous Solutions of Polyion–Surfactant Ion Complex Salts and a Nonionic Surfactant

John Janiak,[†,‡] Matija Tomšič,[§] Dan Lundberg,[†,∥] Gerd Olofsson,[†] Lennart Piculell,[†] and Karin Schillén*[,†]

[†]Division of Physical Chemistry, Department of Chemistry, Center for Chemistry and Chemical Engineering, Lund University, P.O. Box 124, SE-221 00 Lund, Sweden

[§]Faculty of Chemistry and Chemical Technology, University of Ljubljana, Aškerčeva 5, SI-1000 Ljubljana, Slovenia

ABSTRACT: Water-soluble aggregates based on two polyion–surfactant ion "complex salts", consisting of hexadecyltrimethylammonium ($C_{16}TA^+$) and polyacrylate (PA^-) with either 25 or 6000 repeating units, with added nonionic surfactant octaethylene glycol monododecyl ether ($C_{12}E_8$) have been investigated. A previous phase study has shown that added $C_{12}E_5$ or $C_{12}E_8$ can solubilize complex salts in aqueous systems, and that increasing the poly(ethylene oxide) chain length of the nonionic surfactant and/or decreasing the polyion length favors dissolution. In this work we report on dynamic light scattering, NMR diffusometry, small-angle X-ray scattering, and isothermal titration calorimetry measurements performed to characterize the solubilized composite aggregates in dilute aqueous solution in terms of size and stoichiometry. It was found that mixed aggregates of polyacrylate, $C_{16}TA^+$ ions, and $C_{12}E_8$, with almost constant stoichiometry, coexist with free micelles of $C_{12}E_8$ at all investigated mixing ratios. The length of the polyion only weakly affects the stoichiometry of the mixed aggregates while strongly affecting their size and water solubility.

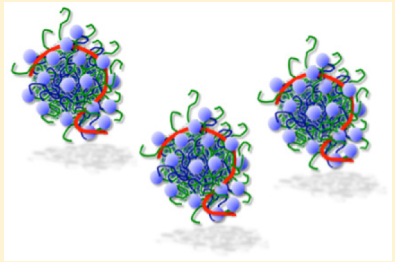

INTRODUCTION

Aqueous mixtures of polyelectrolytes and oppositely charged surfactants are used in many applications, from paints and cleaning agents to foods and pharmaceutical formulations, which have rendered such systems a large scientific interest.[1−8] Several studies have been directed toward the fundamental understanding of the associative phase separation as well as the structures and compositions of the phases formed in such systems.[5,6,8−16] Efforts have also been made to increase the solubility of the aggregates formed by polyion–surfactant ion association in order to expand their applicability to, e.g., drug delivery. One way to achieve an increased solubility is to graft hydrophilic side chains onto the polyion chain or to use diblock copolymers with one polyelectrolyte block and one nonionic block. This will in many cases lead to the formation of soluble or dispersed core–shell nanoparticles, or in some cases vesicles, stabilized by the hydrophilic side chains.[17−24] As an alternative strategy, Dubin et al. have shown that nonionic surfactants can enhance the stability of mixed solutions of polyelectrolytes and oppositely charged surfactants, and they investigated, e.g., the critical conditions at which phase separation occurs.[2−4,25−27] However, most studies that concern aggregation of polyions and oppositely charged surfactant ions have been performed in the presence of simple counterions, which act like an excess salt and thus affect the solubility of the aggregates.[9,13,28]

Previous investigations carried out by our group have utilized so-called complex salts in an attempt to provide a new and simplified way to study oppositely charged polymer–surfactant mixtures in aqueous solution, see, e.g., refs 11,29,30. A complex salt consists of a charged surfactant with an oppositely charged polyion as the sole counterion. This is in contrast to systems where the polyelectrolyte and the surfactant are mixed; in the latter, the simple counterions of the polyion and the surfactant ion are inevitably present and the system consists of four components. By using a complex salt mixed with water and a third component, it is possible to construct a true ternary phase diagram where the effects of excess salt are eliminated. In a recent study we used this approach to investigate the phase behavior in water of two complex salts, based on hexadecyltrimethylammonium ($C_{16}TA^+$) and polyacrylate (PA^-) of different lengths, with added pentaethylene glycol monododecyl ether, $C_{12}E_5$ or octaethylene glycol monododecyl ether, $C_{12}E_8$.[31] The nonionic surfactant was found to strongly partition into the complex salt aggregates, which led to solubilization of the aggregates in certain composition ranges and, also, a rich phase behavior with a multitude of liquid crystalline phases. Recently, we used the knowledge of the phase behavior in one of these complex salt/nonionic surfactant/water systems to prepare thermoresponsive nanoparticles with a bicontinuous cubic internal structure that also show a notable time stability.[32]

In the present study we investigate properties of the soluble aggregates and the aggregate–aggregate interactions in dilute aqueous one-phase solutions of two complex salts where the third component, which gives rise to the aggregate solubility, is the nonionic $C_{12}E_8$ surfactant. Both complex salts are composed of $C_{16}TA^+$ and PA^- but differ in terms of the length of the polyion (polymerization degree, n = 25 or 6000), and

Received: November 28, 2013
Revised: June 8, 2014
Published: June 9, 2014

   dx.doi.org/10.1021/jp411701g | J. Phys. Chem. B 2014, 118, 9745−9756

both are insoluble in water. The composite aggregates formed in water are investigated using isothermal titration calorimetry (ITC), nuclear magnetic resonance diffusometry (NMR diffusometry), dynamic light scattering (DLS), and small-angle X-ray scattering (SAXS). We are thus able to highlight the effects of added $C_{12}E_8$ on structures formed and interactions in the complex salt systems without interference from other ions, that is, at a maximum strength of the electrostatic attraction between polyions and surfactant ions. In particular we are interested in the sizes and stoichiometries of the soluble aggregates that exist in these mixtures. The answers to these questions give insights into mixed aggregate formation in general, and the requirements for solubility of the mixed aggregates in particular.

EXPERIMENTAL SECTION

Material. The nonionic surfactant octaethylene glycol monododecyl either ($C_{12}E_8$ with a nominal molar mass of 538.75 g mol^{-1} and a purity >98%) was purchased from Nikko Chemicals Co., Ltd., and used without further purification. The cationic surfactants hexadecyltrimethylammonium bromide and hexadecyltrimethylammonium chloride, C_{16}TABr and C_{16}TACl (both of p.a. quality), were purchased from Sigma-Aldrich and Tokyo Chemical Industry, respectively. C_{16}TABr was ion exchanged (see below) using MONOSPHERE DOWEX (OH) 550 ion-exchange resin from Sigma-Aldrich whereas C_{16}TACl was used without further purification. Two samples of poly(acrylic acid), PAA, with the molar masses 1800 g mol^{-1} (PAA_{25}) and 450000 g mol^{-1} (PAA_{6000}) were purchased from Sigma-Aldrich. Both samples were dialyzed against water using membranes from Spectrum Laboratories with cutoff MWs of 500 and 10000 respectively, in order to remove low molar mass fractions before use. All solutions were prepared with water purified using a Milli-Q system (Millipore Corporation, Bedford, MA.) except for those used in the NMR experiments. They were prepared with D_2O (99.8 atom % D) purchased from ARMAR Chemicals.

Complex Salts. $C_{16}TAPA_{25}$ and $C_{16}TAPA_{6000}$ were prepared according to a previously developed procedure.[11] In brief, C_{16}TABr was first ion-exchanged to its hydroxide salt (C_{16}TAOH) according to a previously used method,[33] whereafter a reference titration of poly(acrylic acid) was performed to find the pH at the equivalence point. The complex salt was prepared by titration of C_{16}TAOH with a solution of either PAA_{25} or PAA_{6000} to the previously established equivalence point. As a result, a charge-stoichiometric salt containing $C_{16}TA^+$ with polymeric counterions was obtained as a precipitate. The slurry was freeze-dried, and the dry product was stored in a desiccator. Elemental analysis was performed on the complex salts to ensure 1:1 charge stoichiometry. The complex salts are hygroscopic, and despite storage in desiccator over silica gel, a water uptake of about 10 wt % was detected by weighing the sample before and after storage over the absorbent Sicapent (phosphorus pentoxide). This agrees with previous observations.[11]

Sample Preparation. $C_{16}TAPA_{25}$–$C_{12}E_8$ and $C_{16}TAPA_{6000}$–$C_{12}E_8$ samples used for the ITC and SAXS experiments were prepared by weighing 2.51 to 3.22 mg of complex salt, to which 2.6–3.2 mL of water was added. The SAXS samples were transparent monophasic solutions obtained by addition of various amounts of 0.37 M $C_{12}E_8$ stock solution to dissolve the complex salts. NMR-diffusion measurements were performed on dilute water (D_2O) solutions that were prepared with a constant $C_{12}E_8$ concentration, c_{C12E8}, and a varying $C_{16}TAPA_{25}$ or $C_{16}TAPA_{6000}$ concentration. The concentration of complex salt is given in terms of the concentration of $C_{16}TA^+$, c_{C16TA+}, that is, the concentration of repeating units of the complex salt. Concentrations are throughout this paper expressed in mM (= 10^{-3} mol L^{-1}). When preparing solutions, the compositions were corrected for the 10 wt % of water in the complex salts (see above). The complex salts used in the NMR measurements were freeze-dried before use in order to obtain a dry sample to minimize the HDO signal in proton NMR. For DLS, samples with a constant $C_{12}E_8/C_{16}TA^+$ molar ratio (MR = n_{C12E8}/n_{C16TA+}) but varying total concentration ($c = c_{C12E8} + c_{C16TA+}$) were prepared as well as samples with a constant concentration of $C_{12}E_8$ but varying concentration of complex salt. For the $C_{16}TAPA_{25}$ system the investigated molar ratios are 3.5, 6.8, 8.8, 10.7, 21.4, 34.2, and 65.5, whereas for the $C_{16}TAPA_{6000}$ system they are 7.4, 8.9, 11.3, 18.0, 32.9, 47.7, 67.9, and 121.5. The samples with lower MR were prepared by dilution of the more concentrated ones. The stock solutions of pure $C_{12}E_8$ as well as water used for dilution of the samples were filtered using sterile hydrophilic Minisart filters (Sartorius, Germany) with a 0.20 μm in pore diameter.

Isothermal Titration Calorimetry. The titration calorimetric measurements were made at 25 °C using the 2277 TAM Thermal Activity Monitor system (Thermometric AB, Järfälla, Sweden). The experiments consisted of series of consecutive additions of 0.37 M $C_{12}E_8$ solution in portions of 4–15 μL from a gastight Hamilton syringe to the calorimeter vessel initially containing between 4 and 8 mg of solid sample and 2.7 g of water. The samples of the complex salt were sieved to give particles with a diameter of 0.6 mm or less, and as the hydration of the samples was slow, the mounted calorimeter vessel was left overnight to equilibrate. The time between each injection was 120 min for the complex salt samples and 55 min for C_{16}TACl. A microprocessor-controlled motor-driven syringe drive was used for the injections. For more information on the general design of the experiments, see, e.g., ref 34.

Dynamic Light Scattering. The DLS measurements were performed on an ALV/DLS/SLS-5022F, CGF-8F based compact goniometer system from ALV-GmbH., Langen, Germany, equipped a 22 mW He–Ne laser operating at a wavelength (λ) of 632.8 nm, two matched avalanche photodiodes placed in a pseudo-cross geometry, and an ALV-7004 multiple tau digital correlator of 4 × 312 channels covering ≈12 decades in lag time, t. A more detailed description of the instrumentation can be found in ref 32 with the difference that toluene instead of *cis*-decahydronaphthalene is used as refractive-index-matched liquid in the thermostated quartz container (VAT) in which the cylindrical scattering cells of borosilicate glass (10 mm i.d.) are immersed. In this study the measurements were carried out in a vertical-unpolarized geometry with the polarizer located, before the focusing lens, in front of the VAT. The temperature was fixed to 25.0 °C and was controlled to an accuracy of ±0.1 °C using a F32 Julabo heating circulator. Unless otherwise stated the measurements were performed at a single scattering angle $\theta = 90°$.

In the DLS experiment, a time-correlation function of the scattered intensity $G^{(2)}(t)$ (here in pseudo-cross-correlation mode) with an initial real sampling time of 25 ns is measured[35] and its normalized form $g^{(2)}(t)$ (or rather $g^{(2)}(t) - 1$) is provided directly from the software of the correlator. $g^{(2)}(t)$ is related to the normalized time-correlation function of the

dx.doi.org/10.1021/jp411701g | J. Phys. Chem. B 2014, 118, 9745–9756

electric field, $g^{(1)}(t)$, according to $g^{(2)}(t) - 1 = \beta|g^{(1)}(t)|^2$,[36−38] where β (≤ 1) is a coherence factor taking into account the deviations from ideal correlation and experimental geometry. For translational diffusion processes in dilute solution, $g^{(1)}(t)$ (and thereby $g^{(2)}(t) - 1$) is an exponentially decaying function (single, double, or multiexponential) with characteristic relaxation time/times, τ, from which the mutual (or collective) diffusion coefficients D_m for each type of scattering species can be derived. In the case of several decays, $g^{(1)}(t)$ can be expressed as the Laplace transform of the distribution function of relaxation rates $w(\Gamma)$ or relaxation times, $A(\tau)$:[39]

$$g^{(1)}(t) = \int_0^\infty w(\Gamma)\exp(-\Gamma t)\,d\Gamma = \int_{-\infty}^{\infty} \tau A(\tau)\exp(-t/\tau)\,d\ln\tau \quad (1)$$

with $\int_{-\infty}^{\infty}\tau A(\tau)\,d\ln\tau = 1$ and where $\Gamma \equiv 1/\tau$ denotes the rate of the relaxation process. Γ is obtained from the first moment of the relaxation time distribution.

The data analysis was performed with respect to the intensity correlation function using two different techniques: first, by nonlinear regularized inverse Laplace transformation (RILT) in order to retrieve the relaxation time distribution (here presented as $\tau A(\tau) = \log(\tau/\mu s)$ for equal-area representation).[39] This was done using the Regularized Positive Exponential Sum (REPES) algorithm, which operates directly on the $g^{(2)}(t) - 1$ function and minimizes the sum of the squared differences between the experimental and the calculated $g^{(2)}(t) - 1$ functions.[39,40] The smoothing factor *probability-to-reject* was set to 0.5 in all analyses. This factor makes the REPES analysis more robust to artifacts caused by noise than most other analysis techniques. The data obtained from systems containing $C_{16}TAPA_{6000}$ were analyzed using RILT. This was due to the biexponential nature of the intensity correlation functions. Double exponential fits gave similar output, however we chose to present REPES analyses with the accompanying relaxation time distributions, where the mutual diffusion coefficients were evaluated from the two values of relaxation time. In the case of the data on the $C_{16}TAPA_{25}$−$C_{12}E_8$ system, analysis was also made by fitting $g^{(2)}(t) - 1$ to a single exponential function with a baseline B and the coherence factor β (defined above) as adjustable parameters:

$$g^{(2)}(t) - 1 = \beta\exp(-2\Gamma t) + B \quad (2)$$

The mutual diffusion coefficient is defined in the limit of small scattering vectors as

$$D_m = \left(\frac{\Gamma}{q^2}\right)_{q\to 0} \quad (3)$$

where q is the magnitude of the scattering vector, $q = (4\pi n/\lambda)\sin(\theta/2)$, θ is the scattering angle, and n is the refractive index of the solution, which for dilute solutions can be taken to be the refractive index of the solvent.

For all systems investigated in this study, the relaxation rates, according to measurements performed at different angles, were linearly dependent on q^2 through the origin, thus marking a translational diffusion process. D_m may therefore be directly calculated from measurements performed at $\theta = 90°$.

D_m varies linearly with the concentration of the solute (c_{solute}) in the dilute concentration regime, according to[41−43]

$$D_m = D_{m,0}(1 + k_D c_{solute}) \quad (4)$$

where $D_{m,0}$ is the diffusion coefficient at infinite dilution and k_D is hydrodynamic virial coefficient that incorporates both thermodynamic and hydrodynamic factors:[41] $k_D = 2A_2M_w - k_f - 2\bar{v}$, where A_2 is the second virial coefficient, which gives information about the thermodynamic interactions in the system, M_w is the molecular weight of the solute, k_f is the friction coefficient, and $\bar{v}$ is the partial specific volume of the solute. The concentration dependence of the friction coefficient, reflected in the slope k_f, is due to an increased obstruction between the solute particles as the concentration increases (i.e., hydrodynamic excluded volume effects). The factor $(1 - c_{solute}\bar{v})^2$, which has been corrected by Vink,[42] has been omitted in the calculations of D_m since it only becomes important in concentrated solutions.

Nuclear Magnetic Resonance. The NMR diffusometry measurements were performed on a Bruker DMX 200 spectrometer equipped with a Bruker DIFF-25 pulsed field gradient probe. The temperature was set to 25 °C. Spin−echo and stimulated-echo methods were employed for the $C_{16}TAPA_{25}$ and $C_{16}TAPA_{6000}$ systems, respectively.[44,45] The decay of the echo intensity of the signals at 3.72 ppm from the oligo(ethylene oxide) (EO) group of $C_{12}E_8$ and at 3.18 ppm from the trimethylammonium group of $C_{16}TA^+$ was monitored as a function of the strength of the magnetic field gradient in order to determine the average molecular self-diffusion coefficients of $C_{12}E_8$, $D^{C12E8}_{self,obs}$ and $C_{16}TA^+$, $D^{C16TA+}_{self,obs}$. The decay of the echo intensities, $I(b)$, was fitted to a single exponential function:[44,45]

$$I(b) = I_0\exp(-bD_{self,obs}) \quad (5)$$

where $D_{self,obs}$ is the self-diffusion coefficient, b is the diffusion-weighted factor defined as $b = (\gamma G\delta)^2(\Delta - \delta/3)$, where γ is the gyromagnetic ratio of the nucleus that is probed, in this case H^1 ($\gamma = 26.75 \times 10^7$ T^{-1} s^{-1}), G is the strength of the magnetic field gradient in T, δ is the time of the gradient pulse (in this case 0.7 ms), and Δ is the time between two gradient pulses, in this case 50 ms. Finally, I_0 is the intercept for $b = 0$, i.e., the intensity in the absence of field gradients.

In some cases overlap of NMR signals was observed, and a double exponential fit was then used according to

$$I(b) = I_0(A\exp(-bD^1_{self,obs}) + (1 - A)\exp(-bD^2_{self,obs})) \quad (6)$$

where A is the fraction of the contribution of the first exponent to the echo decay. $D^1_{self,obs}$ and $D^2_{self,obs}$ are the self-diffusion coefficients of the two different species.

Small Angle X-ray Scattering. SAXS scattering measurements were performed with a SAXSess camera[46] (Anton-Paar, Graz, Austria), which was attached to a X-ray generator Philips PW3830 operating at 40 kV and 50 mA. A sealed-tube with Cu anode and Göbel mirror was used to produce a focused monochromatic line-shaped beam of Cu Kα radiation (λ = 0.154 nm). The samples were measured in a standard 1 mm thick quartz capillary (wall thickness of 10 μm), which was thermostated at 25 °C. The 2D scattering pattern was recorded by a PI-SCX fused fiber optic taper CCD Camera (pixel size of 24 × 24 μm) from Princeton Instruments, a division of Roper Scientific, Inc. (Trenton, NJ, USA). For each sample, 12 subsequent measurements of 5 min each were made. Cosmic ray correction and CCD background subtraction was performed on the 2D images, which were further reduced

dx.doi.org/10.1021/jp411701g | J. Phys. Chem. B 2014, 118, 9745−9756

into one-dimensional scattering curves and averaged. Such averaged scattering curves were then corrected for the solvent and background scattering and put on absolute scale utilizing water as a secondary standard.[47] However, the resulting scattering curves $I(q)$, where q represents the magnitude of the scattering vector [here defined as $q = (4\pi/\lambda)\sin(\theta/2)$], were still experimentally smeared due to the finite dimensions of the primary X-ray beam.[48] SAXS curves were obtained in the regime 0.07 $nm^{-1} < q < 6$ nm^{-1}.

The SAXS data were evaluated using the Generalized Indirect Fourier Transformation GIFT software package.[49−54] In our study, it was sufficient to use solely its basic part, namely, the Indirect Fourier Transformation method IFT,[55−57] since, due to the low concentrations of the scattering particles in our samples, the interparticle interactions can be neglected. IFT is a completely model-free method, which is only appropriate to employ for dilute particle systems with negligible interparticle interactions. It is based on the fact that the form factor, $P(q)$, which represents the intraparticle scattering contribution, can be written as the Fourier transformation of the pair-distance distribution function $p(r)$:[48,55,56]

$$P(q) = 4\pi \int_0^\infty p(r)\frac{\sin(qr)}{qr}\,\mathrm{d}r \tag{7}$$

where r is the distance between two scattering centers within the particle.

The result of the IFT analysis is the $p(r)$ function, which serves as a tool for the determination of the geometry of the scattering particles.[48,56]At distances r larger than the maximum dimension of particle, the $p(r)$ function adopts the value of zero and provides a useful tool for determination of the maximum dimension of the scattering particles. In addition, the particle symmetry can be deduced from the shape of this function.[48] The scattering contrast profile $\Delta p(r)$ of the scattering particles, which gives valuable information on their internal structure, can be calculated from the $p(r)$ function by a convolution square root operation using the DECON program.[56] Note that r in $p(r)$ corresponds to the distance in the real space (information on the overall size of the scattering particle) but in the radial electron density profile it corresponds to the radius of the scattering particle.

RESULTS AND DISCUSSION

Visual Inspection. Samples of similar compositions as those used in the isothermal calorimetry experiments described below were visually inspected to establish the dissolution efficiency of $C_{12}E_8$. The pure complex salts, $C_{16}TAPA_{25}$ and $C_{16}TAPA_{6000}$, are both insoluble in water. The investigation showed that a mixture of $C_{16}TAPA_{25}$ with a corresponding $C_{16}TA^+$ concentration of 2.8 mM in water was dissolved at a $C_{12}E_8/C_{16}TA^+$ molar ratio in the interval 3.3−3.5, whereas the same concentration of $C_{16}TAPA_{6000}$ required a molar ratio MR of ca. 5.1−6.6. These numbers are in accordance with the previously performed phase study.[31] The phase-separated samples showed either a macroscopic phase separation, containing liquid crystalline phases in equilibrium with a dilute liquid phase, or, close to the dissolution, a turbid appearance.

Isothermal Titration Calorimetry. Figure 1 presents a calorimetric titration curve from small consecutive additions of 0.37 M $C_{12}E_8$ solution to $C_{16}TAPA_{25}$ complex salt, with a corresponding $C_{16}TA^+$ concentration of 1.3 mM, dispersed in water at 25.0 °C. For comparison, the corresponding curve

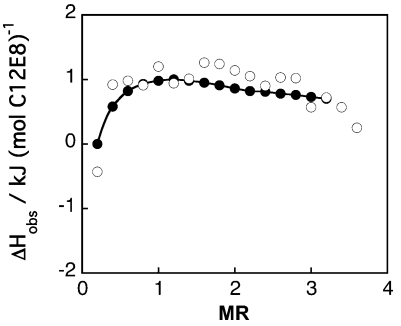

Figure 1. Titration curves for addition of 0.37 M $C_{12}E_8$ solution to an aqueous suspension of $C_{16}TAPA_{25}$ complex salt with a corresponding $C_{16}TA^+$ concentration of 1.3 mM (open symbols) or to 7.1 mM $C_{16}TACl$ in aqueous solution (filled symbols) at 25 °C. Observed enthalpy changes expressed per mole of added $C_{12}E_8$ are plotted against the $C_{12}E_8/C_{16}TA^+$ molar ratio, MR. The solid line is a guide to the eye.

obtained by addition of 0.37 M $C_{12}E_8$ solution to a 7.1 mM micellar solution of $C_{16}TACl$ is also included in Figure 1. The reason for the use of different concentrations of the complex salt and $C_{16}TACl$ is that the comparison is based on $C_{12}E_8/C_{16}TA^+$ molar ratios.

The purpose of the ITC measurements was to compare the $C_{16}TAPA_n/C_{12}E_8$ system with the simpler and previously studied $C_{16}TACl/C_{12}E_8$ system, where mixed micelles are known to form.[58] The calorimetric titration curves presented in Figure 1 are nearly identical for the $C_{16}TACl$ solution and the complex salt systems, which points to the formation of similar mixed micelles with the nonionic surfactant in both cases. We note that the measured exothermic enthalpy changes (with an estimated error of ±0.01 and ±0.1 kJ/mol $C_{16}TA^+$ for the $C_{16}TACl$ and the complex salt system, respectively) are small, which indicates a process mainly driven by entropy. This is consistent with the formation of mixed micelles between ionic and nonionic surfactants, which in general displays quite weak attractive interactions within the micelle.[58]

The complex salt with the long polyion, $C_{16}TAPA_{6000}$, was more difficult to study by titration calorimetry as the equilibration time after addition of $C_{12}E_8$ was found to be long. It was also impossible to reach dissolution with the quantities of complex salt used (see Experimental Section) due to the small volume of the reaction vessel of the calorimeter; the volume of 0.37 M $C_{12}E_8$ solution needed to dissolve $C_{16}TAPA_{6000}$ would overflow the vessel. However, initial measurements suggest that also in this case the enthalpy change is very small, which points to a similar behavior as for $C_{16}TAPA_{25}$. To decrease the amount of $C_{16}TAPA_{6000}$ in order to reach dissolution at smaller additions of $C_{12}E_8$ was not feasible due to the small enthalpy changes.

Reference System of Pure $C_{12}E_8$ Micelles. DLS and NMR Diffusometry. Dynamic light scattering and NMR diffusometry measurements were performed at 25.0 °C on dilute aqueous reference solutions of $C_{12}E_8$. The surfactant concentration (above the critical micelle concentration, cmc, 0.071 mM[59]) was varied from 3.7 to 37.1 mM and from 12.7 to 63.3 mM for DLS and NMR, respectively. In the DLS experiments, the relaxation times were evaluated by using nonlinear regularized inverse Laplace transformation analysis of the single exponential intensity time correlation functions, and the corresponding mutual diffusion coefficients D_m measured at $\theta = 90°$ were calculated using eq 3. The NMR data showed

dx.doi.org/10.1021/jp411701g | J. Phys. Chem. B 2014, 118, 9745−9756

single-exponential behavior and was analyzed using eq 5 to give the self-diffusion coefficients, $D_{self,obs}^{C12E8}$.

In Figure 2, D_m^{C12E8} from DLS and $D_{self,mic}^{C12E8}$ from NMR are presented as functions of surfactant concentration. As noticed,

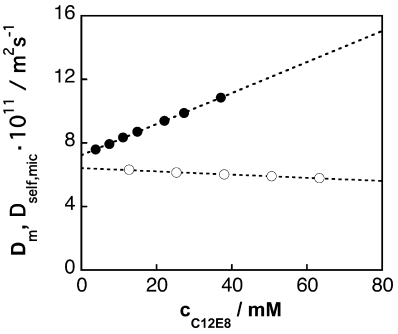

Figure 2. Mutual diffusion coefficients D_m from DLS measured at θ = 90° (filled symbols) and the self-diffusion coefficients $D_{self,mic}$ from NMR (open symbols) of $C_{12}E_8$ aqueous solutions as functions of the $C_{12}E_8$ concentration at 25 °C. For the DLS data each point corresponds to three consecutive measurements, and the estimated standard deviations (std) are smaller than the symbol size and vary between 0.03×10^{-11} and 0.3×10^{-11} m^2 s^{-1}. The dashed lines correspond to linear least-squares fits to the data (the fit to the DLS data is weighted with the std values).

almost perfectly linear relationships were found for both data sets. The negative slope observed for the NMR data is attributed to increasing obstruction, or excluded volume effects, with increasing concentration. The slope was positive for the DLS data, as expected for a system with intermicellar repulsion. A k_D value (see eq 4) of 97.6 M^{-1} was obtained from the linear least-squares fit of the DLS data. The observed diffusion coefficient, $D_{self,obs}^{C12E8}$, is a weighted average because, above the cmc, $C_{12}E_8$ is present both as monomers and in micelles. The NMR data obtained for the micelles has thus been corrected for the influence of the small fraction of rapidly diffusing $C_{12}E_8$ monomers according to

$$D_{self,obs}^{C12E8} = f_{C12E8,mon} D_{self,mon}^{C12E8} + (1 - f_{C12E8,mon}) D_{self,mic}^{C12E8} \quad (8)$$

where $D_{self,mon}^{C12E8}$ and $D_{self,mic}^{C12E8}$ are the self-diffusion coefficients of the $C_{12}E_8$ monomers and the $C_{12}E_8$ micelles, respectively. $f_{C12E8,mon}$ is the fraction of $C_{12}E_8$ present as monomers in the solution and is estimated as the cmc divided by the total concentration. $D_{self,mon}^{C12E8}$ is estimated to be 3.5×10^{-10} m^2 s^{-1}.[59] Using these together with the measured $D_{self,obs}^{C12E8}$ in eq 8, $D_{self,mic}^{C12E8}$ can finally be calculated.

The hydrodynamic radius, R_H, of the $C_{12}E_8$ micelle was estimated from the different diffusion coefficients at infinite dilution D_0 by using the Stokes–Einstein relation: $R_H = kT/6\pi\eta_0 D_0$, where k is Boltzmann's constant, T is the absolute temperature, and η_0 is the viscosity of the solvent (values of 0.890 mPa s and 1.132 mPa s were used for H_2O and D_2O, respectively). R_H values of 3.39 ± 0.02 nm and 3.01 ± 0.01 nm were obtained from DLS and NMR respectively (errors obtained from linear least-squares fits), which is in good agreement with literature data.[60−64] In a related recent study performed in our group, an $R_{H,app}$ of 3.2 nm was estimated from NMR measurements on a solution of 38 mM $C_{12}E_8$ in D_2O.[65]

Complex Salt–$C_{12}E_8$ Systems. NMR Measurements. NMR was employed in order to evaluate the sizes and stoichiometries of the $C_{16}TAPA_n$–$C_{12}E_8$ aggregates at 25.0 °C. The experiments were carried out by varying the concentration of complex salt (expressed as the molar concentration of $C_{16}TA^+$ surfactant ions) in solutions at a constant $C_{12}E_8$ concentration of 40.0 mM. For the $C_{16}TAPA_{25}$ system, the intensity decays of the resonance peak corresponding to EO and trimethylammonium groups, respectively, were fitted to a single exponential function (eq 5). For the $C_{16}TAPA_{6000}$ system, single exponential and a double exponential (eq 6) functions were used for the trimethylammonium and EO decays, respectively. The reason for this is that for the $C_{16}TAPA_{6000}$ system, in contrast to the $C_{16}TAPA_{25}$ system, the trimethylammonium and the EO peaks overlap slightly and also decay at different rates. The results for both complex salts are shown in Figure 3 in order to facilitate a direct comparison.

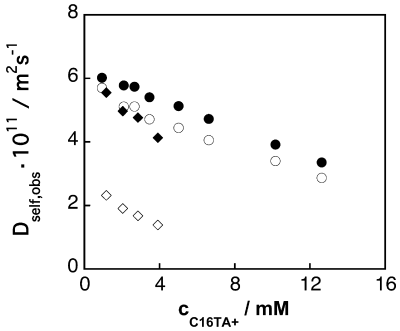

Figure 3. Observed self-diffusion coefficients of $C_{12}E_8$, $D_{self,obs}^{C12E8}$ (filled symbols), and $C_{16}TA^+$, $D_{self,obs}^{C16TA+}$ (open symbols), for increasing concentrations of $C_{16}TAPA_{25}$ (circles) or $C_{16}TAPA_{6000}$ (diamonds) in solutions containing a constant concentration of 40.0 mM $C_{12}E_8$. The temperature was 25 °C.

As can be seen in Figure 3, the self-diffusion coefficients of both surfactants decrease more or less linearly with the complex salt, i.e., $C_{16}TA^+$, concentration. Furthermore, for each complex salt, the diffusion coefficient of $C_{12}E_8$, $D_{self,obs}^{C12E8}$, is larger than the diffusion coefficient of $C_{16}TA^+$, $D_{self,obs}^{C16TA+}$. The difference is relatively small for $C_{16}TAPA_{25}$ but quite large for $C_{16}TAPA_{6000}$. We estimate the errors in $D_{self,obs}^{C12E8}$ and $D_{self,obs}^{C16TA+}$ to be less than 5%. Clearly, the diffusion of the surfactant ions is sensitive to the size of the polyion, being much slower for a large polyion, whereas the diffusion of the nonionic surfactant is much less sensitive. As we shall see, this is because the $C_{16}TA^+$ ions reside essentially only in aggregates of polyions and mixed micelles (henceforth referred to simply as mixed aggregates), whereas there is a substantial, but varying, fraction of $C_{12}E_8$ molecules that are "free", i.e., not bound to the polyions.

Owing to the rapid exchange of $C_{12}E_8$ molecules between three different environments where they can reside, i.e., in the mixed aggregates containing the complex salt, in free $C_{12}E_8$ micelles, and as free monomers, the observed self-diffusion coefficient can be described by the relation[45]

$$D_{self,obs}^{C12E8} = f_{C12E8,agg} D_{self,agg}^{C12E8} + f_{C12E8,mon} D_{self,mon}^{C12E8} + f_{C12E8,mic} D_{self,mic}^{C12E8} \quad (9)$$

where $D_{self,agg}^{C12E8}$, $D_{self,mon}^{C12E8}$, and $D_{self,mic}^{C12E8}$ are the self-diffusion coefficients of mixed aggregates, $C_{12}E_8$ monomers, and $C_{12}E_8$ micelles, respectively, and the corresponding fs are the fractions of $C_{12}E_8$ present in mixed aggregates, monomers, or micelles, respectively.

dx.doi.org/10.1021/jp411701g | J. Phys. Chem. B 2014, 118, 9745−9756

Our next task will be to calculate these various fractions f and their variation with the system composition, using eq 9 and the experimental data in Figure 3. Since (as we shall see) free nonionic micelles are present throughout the experimental composition range, we can assume that the $C_{12}E_8$ monomer concentration equals cmc = 0.071 mM (see above). This is clearly negligible compared to the constant total concentration of 40 mM. Taking as before $D^{C12E8}_{self,mon} = 3.5 \times 10^{-10}$ m^2 s^{-1}, and $f_{C12E8,mon}$ as cmc divided by the total $C_{12}E_8$ concentration (40 mM), we obtain $f_{C12E8,mon}D^{C12E8}_{self,mon} = 6.2 \times 10^{-13}$ m^2 s^{-1}, i.e., the contribution from free monomer *diffusion* is also negligible compared to all observed $C_{12}E_8$ diffusion coefficients in Figure 3. For the diffusion coefficient of a $C_{12}E_8$ micelle $D^{C12E8}_{self,mic}$ we use the value 6.1×10^{-11} m^2 s^{-1} obtained for 40 mM $C_{12}E_8$, see Figure 2. Owing to the weak concentration dependence observed in Figure 2, we neglect the additional obstruction to diffusion of the $C_{12}E_8$ micelles that is caused by <13 mM added $C_{16}TA^+$ in the experiments in Figure 3.

Finally, for the mixed aggregate diffusion, we will use, $D^{C12E8}_{self,agg} = D^{C16TA+}_{self,obs}$. The latter assumption requires some additional justification. Strictly, the surfactant ions, like the nonionic surfactant molecules, can reside in three environments: in the mixed aggregates, as dissolved monomeric surfactant ions, or mixed into the free nonionic micelles. This implies an equation for the observed surfactant ion diffusion coefficient completely analogous to eq 9. The concentration of monomeric surfactant ions should be very low, however. As a first estimate, we may use the critical association concentration, cac, of $C_{16}TA^+$ ions binding to polyacrylate in aqueous solution, which has been estimated to be ca. 10^{-6} M.[66] However, one may argue that when nonionic surfactant is mixed into the polyion-bound micelles (as in our study), the concentration of free surfactant ions should decrease even further. With a total $C_{16}TA^+$ concentration ≥1 mM and a diffusion coefficient of ca. 4×10^{-10} m^2 s^{-1} for the monomer surfactant ions,[67] we therefore find that the contribution from diffusing monomeric surfactant ions is negligible compared to all observed $C_{16}TA^+$ diffusion coefficients in Figure 3.

The fraction of $C_{16}TA^+$ mixed in the free nonionic micelles is more difficult to estimate. To obtain a rough estimate, we can use the phase-separation model for mixed micellization assuming ideal mixing in the micellar phase.[68] This model relates the free monomer concentration, $c_{C16TA+,mon}$, to the mole fraction of ionic surfactant in the free micelle, $X_{C16TA+,mic}$, according to $c_{C16TA+,mon} = X_{C16TA+,mic}\cdot cmc_{C16TA+}$. Using, as before, $c_{C16TA+,mon} \approx 10^{-6}$ M, and $cmc_{C16TA+} \approx 10^{-3}$ M (≈cmc of $C_{16}TABr$),[58] we arrive at $X_{C16TA+,mic} \approx 10^{-3}$, giving a maximum concentration of ionic surfactant mixed in the free micelles of $10^{-3} \times 40$ mM = 0.04 mM. At the lowest $C_{16}TA^+$ concentrations of ca. 1 mM in Figure 3, this would correspond to a fraction of 0.04 of the surfactant ions residing in the free micelles. Multiplying this fraction with a diffusion coefficient of 6.1×10^{-11} m^2 s^{-1} for the free micelles (see above), we finally obtain a contribution to the observed diffusion coefficient, from the surfactant ions residing in the nonionic micelles, of the order of 2×10^{-12} m^2 s^{-1} at the lowest $C_{16}TA^+$ concentration. While this contribution is significant compared to the experimental uncertainty in Figure 3, it corresponds to less than 10% of the measured diffusion coefficients. Based on the above considerations we conclude that our assumption, that the observed $C_{16}TA^+$ diffusion coefficient equals the mixed aggregate diffusion coefficient, is justified.

We are now at the position where we can calculate, for each concentration of complex salt, the fraction (of the total amount) of $C_{12}E_8$ molecules that reside in mixed aggregates with the complex salt. This can be obtained as $f_{C12E8,agg} = 1 - f_{C12E8,mon} - f_{C12E8,mic}$. We will also calculate $X_{C12E8,agg}$, defined as the mole fraction of $C_{12}E_8$ in the $C_{16}TA^+$–$C_{12}E_8$ mixed micelles that appear in the mixed complex salt aggregates ($X_{C12E8,agg} = n_{C12E8,agg}/(n_{C12E8,agg} + n_{C16TA+})$. The results are shown in Figure 4. Before we discuss numbers and trends in Figure 4, we note

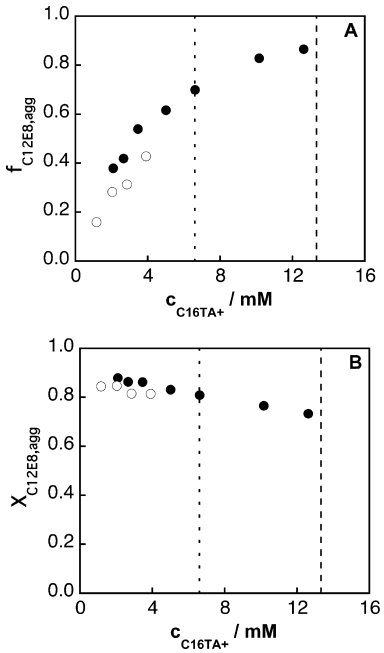

Figure 4. (A) The fraction of $C_{12}E_8$ that resides in mixed aggregates with the complex salt and (B) the mole fraction of $C_{12}E_8$ participating in such mixed aggregates plotted versus the concentration of complex salt in solutions containing a constant concentration of 40 mM $C_{12}E_8$. Data refer to $C_{16}TAPA_{25}$–$C_{12}E_8$ mixtures (filled symbols) or $C_{16}TAPA_{6000}$–$C_{12}E_8$ mixtures (open symbols). The vertical lines represent limits of one-phase solution regions for $C_{16}TAPA_{25}$–$C_{12}E_8$ mixtures (dashed line) and $C_{16}TAPA_{6000}$–$C_{12}E_8$ mixtures (dotted line).

that the values of both $f_{C12E8,agg}$ and $X_{C12E8,agg}$ that emerge from our analysis are quite similar for the two complex salts, lending credibility to the analysis and the underlying assumptions.

Figure 4A shows that the fraction $C_{12}E_8$ (of the total amount) that resides in the mixed aggregates increases substantially with increasing concentration of complex salt: the added complex salt consumes the free micelles and incorporates the nonionic surfactant in the mixed aggregates, in agreement with the conclusion from the ITC measurements. Interestingly, the mole fraction of nonionic surfactant in the mixed aggregates (Figure 4B) is almost constant, although there is a slightly decreasing trend at least for $C_{16}TAPA_{25}$, where $X_{C12E8,agg}$ decreases monotonically from ∼0.85 at low concentration of complex salt to ∼0.75 as the concentration of complex salt increases to 13 mM. Thus, the solubilized complex salts are characterized by a finite fraction of ionic surfactant in the mixed aggregates even at an overwhelming excess of nonionic surfactant; the value of $X_{C12E8,agg}$ does not extrapolate to 1 at zero concentration of complex salt. At the other end of the one-phase region, the mixed aggregates are characterized by a large fraction of nonionic surfactant in the mixed micelles,

dx.doi.org/10.1021/jp411701g | J. Phys. Chem. B 2014, 118, 9745–9756

also close to the phase boundary. Interestingly, a significant fraction of pure $C_{12}E_8$ micelles coexists with the mixed aggregates even at the phase boundary, and the fraction of nonionic micelles at the phase boundary is particularly large for the complex with the long polyion.

Having established the existence, the stoichiometries, and the concentrations of two distinct types of particles, i.e., mixed complex salt−$C_{12}E_8$ aggregates and pure nonionic $C_{12}E_8$ micelles, in the solutions of solubilized complex salts, we will now turn to the properties of the mixed aggregates, starting with the ones formed for $C_{16}TAPA_{25}$. The finite fraction of ionic surfactant in the micelles already at low concentration of complex salt is consistent with the requirement that an entire unit of complex salt, i.e., one polyion and its ca. 25 $C_{16}TA^+$ counterions, has to be incorporated in a mixed aggregate. Comparing Figures 2 and 3 we note that (1) at low concentrations of complex salt, the complex salt aggregates diffuse almost as rapidly as the pure nonionic micelles, but (2) the observed self-diffusion coefficient $D_{self,obs}^{C12E8}$ decreases much more strongly with added complex salt (Figure 3), compared to the effect on $D_{self,mic}^{C12E8}$ of instead adding more nonionic surfactant above 40 mM, see Figure 2 (this was confirmed by a plot of the combined data in Figures 2 and 3 as a function of volume fraction, not shown). The latter comparison leads us to the conclusion that the excluded volume of the added complex salt is not the cause of the decrease of the diffusion coefficient of the mixed aggregates; rather, this trend should be a result of aggregate growth. From the data in Figure 3 we may calculate, through the Stokes−Einstein relation, the apparent hydrodynamic radius, $R_{H,app}$, of the mixed aggregates in the solutions containing a constant concentration of 40.0 mM $C_{12}E_8$. We find that $R_{H,app}$ varies between 3.4 and 6.8 nm at the lowest and at the highest $C_{16}TA^+$ concentration, respectively.

We see two different possible ways in which the mixed aggregates may grow: Either (1) a growth of the $C_{16}TA^+$−$C_{12}E_8$ mixed micelles into elongated or wormlike micelles, accompanied by the incorporation of additional PA_{25}^- polyions bound to each surfactant micelle, or (2) an agglomeration of small (spherical or nearly spherical) micelles into larger clusters, which are held together by the polyanions. The experimental data *per se* do not allow us to decide which of these two possible scenarios is the most likely (one may have a combination of both), but we find some circumstantial arguments that would favor the second explanation. We argue above that a complex salt entity of one short polyion (25 repeating units) and its 25 counter-surfactant ions should be incorporated in its entirety in a mixed complex salt−$C_{12}E_8$ aggregate. If we imagine this to be a single micelle with the same aggregation number as a $C_{12}E_8$ micelle (90−120 at ambient temperatures[69]), we would obtain an average mole fraction of ∼0.21−0.28 of ionic surfactant in the mixed micelle ($1-X_{C12E8,agg}$), which is larger than the fraction of ionic surfactant in a mixed aggregate obtained in Figure 4B. It is conceivable, however, that it is more favorable for a complex salt unit to share its surfactant ions between two micelles than to have them all collected in a single micelle. This would increase the entropy of mixing of the surfactant ions, and also allow a more efficient packing of the latter around the polyion, which has a quite high linear charge density (a charge−charge separation of 0.25 nm in the chain). A preferred sharing of the surfactant ions in a $C_{16}TAPA_{25}$ complex salt unit between two micelles would lead to a net attraction between mixed micelles, a bridging effect. This would, in turn, provide an explanation for the observed decrease in $X_{C12E8,agg}$ with increasing complex salt concentration (Figure 4B) in terms of an increasing fraction of polyion cross-linkers per micelle in the multimicellar aggregates.

The trends for the $C_{16}TAPA_{6000}$−$C_{12}E_8$ system are similar to those observed for the $C_{16}TAPA_{25}$−$C_{12}E_8$ system. However, the self-diffusion coefficient of the mixed aggregates is smaller due to larger aggregate size as a consequence of the longer PA_{6000}^- polyion. The difference in apparent size of the aggregates ($R_{H,app}$ is 16.2 nm at the highest and 8.3 nm at the lowest $C_{16}TA^+$ concentration) can be explained similarly as for $C_{16}TAPA_{25}$−$C_{12}E_8$ system as an increased aggregation.

As a final remark, the increased propensity for aggregation as the phase boundary is approached gives a physical explanation of the phase separation that eventually occurs on addition of complex salt. When the mixed aggregates reach a certain size, the system separates into one dilute phase, containing mostly nonionic micelles, and one concentrated micellar phase, enriched in the large mixed aggregates.[31]

Complex Salt−$C_{12}E_8$ Systems. DLS Measurements. The complex salt−$C_{12}E_8$ solutions were studied by dynamic light scattering at 25 °C. In this section, we prefer to present and discuss the results for the complexes with the short and the long polyions separately, beginning with the results for the short polyion.

$C_{16}TAPA_{25}$−$C_{12}E_8$ System. All relaxation time distributions obtained from nonlinear regularized inverse Laplace transformation (using the REPES program) of the intensity time correlation functions for the $C_{16}TAPA_{25}$ system with $C_{12}E_8$ were monomodal in the investigated $C_{12}E_8/C_{16}TA^+$ molar ratio range 3.5 to 65.5 (above the boundary of dissolution of $C_{16}TAPA_{25}$). Figure 5 shows one example. As discussed above,

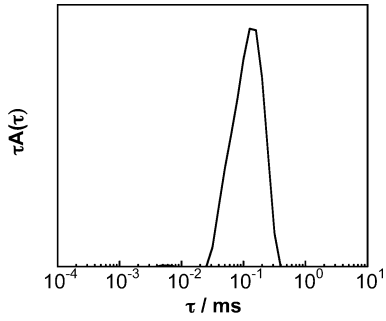

Figure 5. Relaxation time distribution from regularized inverse Laplace transformation of the intensity correlation function of $C_{16}TAPA_{25}$−$C_{12}E_8$ aqueous solution containing 70.0 mM $C_{12}E_8$ and 19.9 mM of $C_{16}TA^+$ (MR = 3.5) at 25 °C.

the NMR experiments clearly indicated that both mixed complex salt−$C_{12}E_8$ aggregates and free $C_{12}E_8$ micelles exist in this MR range. It becomes evident from Figure 5 that the DLS technique is unable to separate the mutual diffusion of these two species; the distribution is distorted and quite broad, which also indicates a size polydispersity. This is consistent with the reported mutual diffusion coefficients' containing contributions from two different classes of diffusing particles (nonionic micelles and mixed aggregates of varying size).

The dependence of the total concentration ($c = c_{C16TA+} + c_{C12E8}$) on the mutual diffusion coefficient was investigated at various $C_{12}E_8/C_{16}TA^+$ molar ratios (Figure 6). We observe that, for all cases, D_m varies linearly with the total concentration, indicating that at a constant MR the size (i.e.,

dx.doi.org/10.1021/jp411701g | J. Phys. Chem. B 2014, 118, 9745−9756

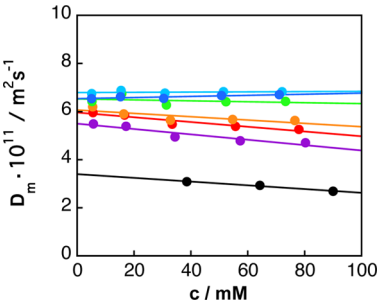

Figure 6. Mutual diffusion coefficient as a function of the total concentration of $C_{16}TAPA_{25}$ and $C_{12}E_8$ ($c = c_{C16TA+} + c_{C12E8}$) for various $C_{12}E_8/C_{16}TA^+$ molar ratios at 25 °C: MR = 3.5 (black), MR = 6.8 (purple), MR = 8.8 (red), MR = 10.7 (orange), MR = 21.4 (green), MR = 34.2 (light blue), and MR = 65.5 (blue). The scattering angle is 90°. The estimated errors (between 0.5 and 5%) are smaller than the size of the symbols. The lines correspond to linear least-squares fits to the data.

mean size of nonionic micelles and mixed aggregates) is essentially unchanged in this concentration regime. From almost no or a weak concentration dependence for the two solutions with the highest molar ratios (65.5 and 34.2), the slope changes and becomes increasingly negative as the $C_{12}E_8/C_{16}TA^+$ molar ratio decreases. The slopes (i.e., the k_D values, see eq 4) are (from high to low MR) 2.3, 0.5, −2.0, −6.9, −9.9, −11.1, and −7.8 M^{-1}. This reflects that the interaction in the system changes depending on the molar ratio of nonionic surfactant to $C_{16}TAPA_{25}$. The slope involves both thermodynamic and hydrodynamic terms ($k_D = 2A_2M_w - k_f - 2\bar{v}$, see eq 4).[41] If M_w, $\bar{v}$, and A_2 are independent of concentration, the sign of k_D depends on the magnitude of A_2. If the pair interactions are repulsive ($A_2 > 0$), then k_D is positive and the mutual diffusion coefficient increases with total concentration. A negative slope signals an approach to the theta solvent condition [$k_D = -(k_f + 2\bar{v})$ for $A_2 = 0$] and also that an attractive contribution to the interactions is present. In the $C_{16}TAPA_{25}$−$C_{12}E_8$ system, we can thus conclude that, at high MR, there is a weak repulsion between the particles, which between MR = 20 and MR = 40 changes to an attractive interaction as evidenced by the change to a slightly negative slope. The repulsive average interaction in the high molar ratio regime may be coupled to the increasing concentration of free $C_{12}E_8$ micelles. It can be noticed that the k_D values found for the solutions with high MR are far below the value of pure $C_{12}E_8$ micelles (97.6 M^{-1}), which indicates that the interactions are much less repulsive in the $C_{16}TAPA_{25}$−$C_{12}E_8$ system even with high excess of nonionic surfactant. The fact that the interaction becomes attractive with decreasing MR is consistent with the proposed model of clustering of spherical micelles by polyanions (model 2, above.)

The hydrodynamic radius at infinite dilution can be evaluated from the intercept of the linear relation given in eq 4 (i.e., from $D_{m,0}$). It should be remembered that this value is an average of the radii of the two species in solution, i.e., the mixed complex salt−surfactant aggregate and the free $C_{12}E_8$ micelle. We find the following R_H values (from high to low MR): 3.8, 3.6, 3.8, 4.1, 4.1, 4.5, and 7.2 nm. These results are consistent with the NMR diffusometry data, which present a decrease in the apparent diffusion coefficient with increasing $C_{16}TA^+$ concentration at a constant nonionic surfactant concentration (compare different MR at a constant total concentration $c = c_{C12E8} + c_{C16TA+}$ in Figure 6).

$C_{16}TAPA_{6000}$−$C_{12}E_8$ System. The complex salt system composed of the long polyacrylate polyion ($C_{16}TAPA_{6000}$) and $C_{12}E_8$ was investigated in the $C_{12}E_8/C_{16}TA^+$ molar ratio range 7.4 to 121.5, which is above the boundary of dissolution for the complex salt. The intensity correlation functions from the DLS measurements of the $C_{16}TAPA_{6000}$−$C_{12}E_8$ solutions were biexponential, and thus the relaxation time distributions obtained from the REPES analyses were bimodal. Figure 7 presents a representative correlation function together with the corresponding relaxation time distribution and a double exponential fit of the latter.

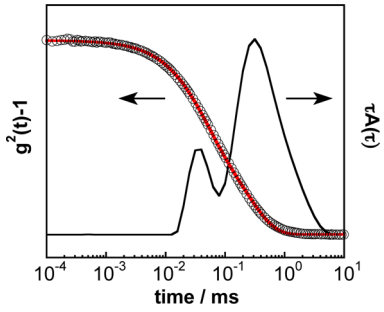

Figure 7. Pseudo-cross correlation function of the scattered light at θ = 90° for $C_{16}TAPA_{6000}$−$C_{12}E_8$ aqueous solution containing 70.0 mM $C_{12}E_8$ and 1.03 mM $C_{16}TA^+$ (MR = 67.9) at 25 °C (circles). Also shown is the relaxation time distribution obtained from regularized inverse Laplace transformation (black solid line) of the correlation function and a fitted double exponential function (red solid line).

We observe that the fast relaxation mode has smaller amplitude than the slow relaxation mode and that the modes are still clearly separated although they partly overlap. At low MR the fast mode contributes only with a few percent to the total intensity of the scattered light. According to the NMR experiments both complex salt systems behave similarly, i.e., mixed complex salt−$C_{12}E_8$ aggregates coexist with free nonionic micelles. Accordingly, the bimodal behavior found in the DLS experiments is a consequence of the coexistence of smaller particles (fast relaxation time) with a considerably larger species (slow relaxation time). The slow mode can be ascribed to the large mixed aggregates of complex salt and nonionic surfactant while the fast mode may originate from the diffusion of free nonionic micelles. The slow mode is broad, which indicates a significant polydispersity in the size of the mixed aggregates. The size difference of the two scattering objects is much larger than in the $C_{16}TAPA_{25}$−$C_{12}E_8$ system, and the mutual diffusion coefficients related to each of them could be then obtained in the DLS measurements. An extrapolation to zero total concentration of the diffusion coefficient, calculated from the fast mode at a high molar ratio (MR = 67.9), gives a hydrodynamic radius of 3.16 nm (data not shown), which is close to the value of pure $C_{12}E_8$ micelles (3.39 nm). It is thus reasonable to suggest that the fast mode can be attributed essentially to free $C_{12}E_8$ micelles.

To allow comparison between DLS and NMR data, the values of D_m of the slow mode are presented in the same way as for the results from NMR diffusometry, i.e., with the $C_{12}E_8$ concentration constant and with a varying the $C_{16}TA^+$ concentration. The apparent mutual diffusion coefficients, which are calculated from the relaxation times of the slow mode at constant $C_{12}E_8$ concentrations (20 mM to 70 mM),

dx.doi.org/10.1021/jp411701g | J. Phys. Chem. B 2014, 118, 9745−9756

are plotted as a function of the $C_{16}TAPA_{6000}$ concentration (expressed as $C_{16}TA^+$ concentration) in Figure 8.

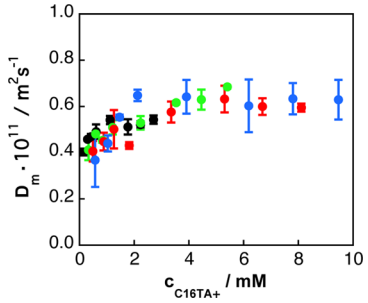

Figure 8. Mutual diffusion coefficients of the slow mode of the $C_{16}TAPA_{6000}$–$C_{12}E_8$ system at 25 °C presented as a function of $C_{16}TA^+$ concentration at constant $C_{12}E_8$ concentration of 20.0 mM (black symbols), 40.0 mM (green), 60.0 mM (red), and 70.0 mM (blue). The error bars are given as ±standard deviation for three sequential measurements. The scattering angle is 90°.

It is noticed that, when comparing the different $C_{12}E_8$ concentration series, the mutual diffusion coefficients obtained at a given $C_{16}TA^+$ concentration do not vary much with the $C_{12}E_8$ concentration. Furthermore, for all series, the diffusion coefficients increase at low $C_{16}TA^+$ concentrations (0–4 mM) and have the dependence expected for a repulsive interacting system. The fact that that a linear relationship is found implies that the average size is constant in this concentration regime. From the NMR experiments, it is observed that the relative fractions of $C_{12}E_8$ and $C_{16}TA^+$ in the complex salt change very little in this low concentration regime (Figure 4B). The $R_{H,app}$ of the mixed $C_{16}TAPA_{6000}$–$C_{12}E_8$ aggregates is 48 nm as calculated from the D_m value of the 40 mM $C_{12}E_8$ series at a low $C_{16}TA^+$ concentration corresponding to MR = 33 (Figure 8). It may be compared to 8.3 nm obtained from NMR at MR = 34 and at 40 mM $C_{12}E_8$ (Figure 3). It can be noted that the diffusion coefficients measured using DLS and NMR diffusometry differed roughly by a factor 2–3. This is not astonishing since the two techniques provide two different weighted averages. DLS gives a *z*- (or intensity-) weighted average whereas NMR gives a mass- (or volume-) weighted average. This difference, in addition to the different effect of the interparticle interactions, does not allow for a strict comparison of the two diffusion coefficients. Above 4 mM $C_{16}TA^+$, the diffusion data seem to level off. At this stage, we should recall that the apparent size of the mixed aggregates increases with increasing $C_{16}TA^+$ concentration according to the NMR data (Figure 3) while the stoichiometry is unchanged (Figure 4B). Hence, we suggest that the lowering (deviation from the linear relationship) of the diffusion coefficients at $c_{C16TA+} > 4$ mM could be a result of the formation of mixed aggregates by a possible bridging of two or several polyions accompanied by an increased attractive interaction as the system approaches phase separation.

$C_{16}TAPA_{25}$–$C_{12}E_8$ System. Small Angle X-ray Scattering Measurements. SAXS experiments were performed at 25 °C on dilute aqueous reference solutions of $C_{12}E_8$ and on $C_{16}TAPA_{25}$–$C_{12}E_8$ and $C_{16}TAPA_{6000}$–$C_{12}E_8$ solutions with various $C_{12}E_8/C_{16}TA^+$ molar ratios. Due to the low concentrations of the scattering particles in the studied samples, the scattering curves were evaluated with the model-free method, indirect Fourier transformation IFT, to yield the resulting pair-distance distribution functions $p(r)$.[55−57]

The experimental SAXS data for the $C_{12}E_8$ solutions with concentrations ranging from 12.6 to 63.1 mM (0.68 to 3.4 wt %) are reported in Figure 9. These concentrations are in the

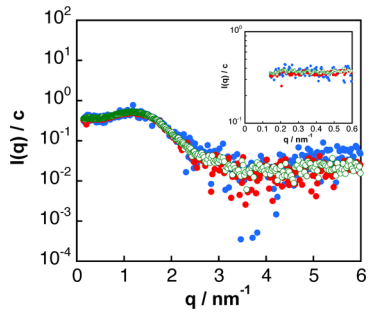

Figure 9. Normalized experimental SAXS curves of $C_{12}E_8$ in water at different concentrations: 12.6 mM (blue filled symbols), 34.0 mM (red filled symbols), and 63.1 mM (green open symbols). Measurements were performed at 25 °C. The inset shows the same data on an enlarged scale.

same concentration range of $C_{12}E_8$ as those used in mixed systems. As can be noticed, the concentration-normalized curves display essentially no difference in the regime of low *q* values (see enlargement), where the effect of interparticle interactions would have the strongest influence. This suggests that the interparticle interactions are similar in all these samples and are also very weak, and the latter fact justifies that these are neglected in the data analysis.

Figures 10A and 10B show the experimental SAXS curves and the corresponding pair-distance distribution functions $p(r)$ for a 12.6 mM $C_{12}E_8$ neat solution and a mixed solution containing $C_{12}E_8$ and $C_{16}TAPA_{25}$ at a MR of 5.6. By assuming a globular shape of the scattering particles based on the resulting $p(r)$ functions, the scattering contrast profile $\Delta\rho(r)$ can be obtained deconvoluting the corresponding $p(r)$ functions. These profiles are presented in Figure 10C.

The scattering peaks observed in Figure 10A are related to the form factor of the free $C_{12}E_8$ micelles and the mixed $C_{16}TAPA_{25}$–$C_{12}E_8$ aggregates, respectively. The position of the scattering peaks slightly shifts toward lower *q* values, indicating that there is a slight increase in the size of the scattering particle when the $C_{16}TAPA_{25}$ complex salt is present in the $C_{12}E_8$ system. Such a size increase of the scattering particles is more clearly observed from the $p(r)$ functions presented in Figure 10B. Furthermore, these functions indicate a similar shape of the scattering particles with their maximum dimension around 7.5 and 8.0 nm for the $C_{12}E_8$ micelles and the particles in the mixed $C_{16}TAPA_{25}$–$C_{12}E_8$ system, respectively. The obtained radius of the $C_{12}E_8$ micelle, i.e., 3.75 nm, agrees well with the R_H value of 3.39 nm obtained from DLS results and from the literature.[62] Furthermore, the radius of the $C_{16}TAPA_{25}$–$C_{12}E_8$ aggregates (4 nm) is comparable to the R_H = 4.5 nm obtained from DLS results of the system with the closest MR = 6.8 and $R_{H,app}$ = 4.8 nm obtained from NMR results at MR = 6. It should be stressed that the obtained maximum dimension of the scattering particles in the $C_{16}TAPA_{25}$–$C_{12}E_8$ system is an average value of the size of the mixed aggregates and the $C_{12}E_8$ micelles (for the same reason as for the values of the hydrodynamic radii from DLS). As shown, this average size is slightly larger than that of the pure nonionic micelles, and it

dx.doi.org/10.1021/jp411701g | J. Phys. Chem. B 2014, 118, 9745−9756

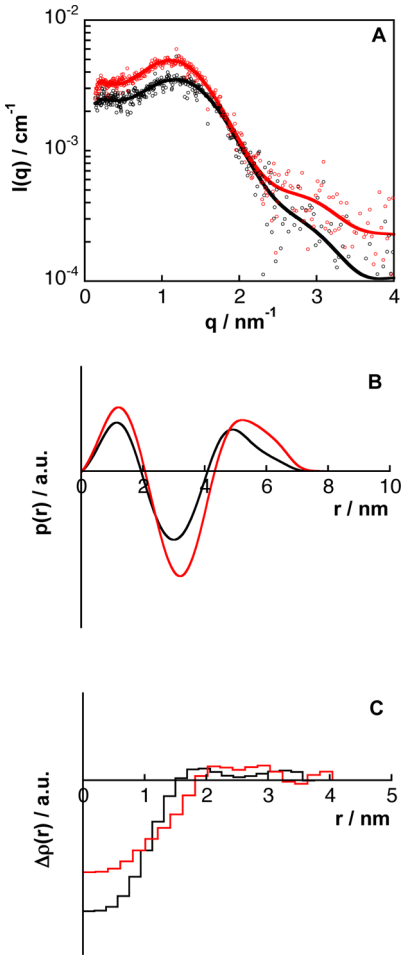

Figure 10. (A) Experimental SAXS curves of a 12.6 mM $C_{12}E_8$ aqueous solution (black symbols) and a mixed $C_{16}TAPA_{25}$–$C_{12}E_8$ solution containing 12.6 mM $C_{12}E_8$ and 2.27 mM $C_{16}TA^+$ (equivalent to MR = 5.6) (red). The solid lines with the same colors as the corresponding data are IFT fits. Measurements performed at 25 °C. (B) Corresponding pair-distance distribution functions. (C) Corresponding excess radial electron density distributions $\Delta\rho(r)$.

cannot be ruled out that mixed aggregates formed by two mixed micelles sharing one polyion, as described above, could exist in the system. However, the SAXS measurements were performed under more dilute conditions compared to the NMR measurements, which could influence the formation of such aggregates. The presented $p(r)$ functions also show that both the micelles and the mixed aggregates are inhomogeneous, as is expected for systems containing core–shell particles.[70] Furthermore, the electron density profiles $\Delta\rho(r)$ displayed in Figure 10C reveal a small difference in the internal structure of the scattering particles in these two cases, which clearly indicates that the complex salt is indeed included in the scattering particles. From the point where these profiles intersect the x-axis at $y = 0$, we obtain the radius of the core of the scattering particle. The core radius of the $C_{12}E_8$ micelles is around 1.6 nm, but for complex salt aggregates it is around 1.9 nm. This is a reasonable change, because the mixed aggregates contain a certain amount of C_{16} chains as compared to only C_{12} chains for the neat $C_{12}E_8$ system. At larger MR, the SAXS curves obtained from the mixed system are essentially indistinguishable from that of $C_{12}E_8$ (data not shown). Nevertheless, we know from NMR diffusometry that nonionic surfactant micelles coexist with mixed aggregates and that the nonionic surfactant will partition between aggregates and micelles also in these systems. Thus, as concentration of $C_{12}E_8$ is increased in the system, the fraction of pure $C_{12}E_8$ micelles increases and eventually prevails in the scattering of these samples. A very similar situation was observed in the SAXS results for the mixed solutions of $C_{16}TAPA_{6000}$ and $C_{12}E_8$, which could only be studied at relatively high MR values (data not shown). Also in this case the scattering curves of pure surfactant and mixed systems were practically the same: the SAXS curves were dominated by the scattering contribution of the free micelles. Taken together, the results from the SAXS investigation are consistent with the results from the other techniques and clearly confirm the formation of mixed $C_{16}TAPA_{25}$–$C_{12}E_8$ aggregates that consist of small spherical mixed micelles.

CONCLUSIONS

When a water-insoluble complex salt composed of $C_{16}TA^+$ surfactant ions and polyacrylate ions is mixed with the nonionic surfactant $C_{12}E_8$, mixed aggregates are formed, and the complex salt eventually becomes completely solubilized at a certain global $C_{12}E_8/C_{16}TA^+$ molar ratio that depends on the length of the polyion (a single solution phase is obtained). In the present study, the size and stoichiometry of the aggregates formed at various global molar ratios in dilute aqueous solutions have been investigated. It was found that mixed $C_{16}TAPA_n$–$C_{12}E_8$ aggregates coexist with free $C_{12}E_8$ micelles at all compositions investigated. At constant concentration of $C_{12}E_8$ and increasing concentration of complex salt, there is a substantial increase in the fraction of $C_{12}E_8$ residing in the mixed aggregates. However, the relative fractions of $C_{12}E_8$ and $C_{16}TA^+$ within the mixed aggregates are practically independent of the global $C_{12}E_8/C_{16}TA^+$ molar ratio, which suggests that the stoichiometry of the mixed aggregates is essentially constant (irrespectively of the length of the polyion). In the $C_{16}TAPA_{25}$–$C_{12}E_8$ system at low $C_{16}TA^+$ concentrations (or high $C_{12}E_8/C_{16}TA^+$ molar ratios), the mixed aggregates, which have a size similar to that of $C_{12}E_8$ micelle, consist of small mixed micelles bound to polyacrylate ions. With increasing concentration of complex salt (or decreasing $C_{12}E_8/C_{16}TA^+$ molar ratios), there is an increase in the size of the mixed aggregates. Most likely, the larger aggregates consist of several small mixed micelles sharing one or more polymeric counterions. The behavior of the $C_{16}TAPA_{6000}$ system is similar to that of the $C_{16}TAPA_{25}$ system except that the mixed $C_{16}TAPA_{6000}$–$C_{12}E_8$ aggregates are considerably larger.

AUTHOR INFORMATION

Corresponding Author

*E-mail: Karin.Schillen@fkem1.lu.se. Tel: +46 46 222 1439.

Present Addresses

‡Akzo Nobel Surface Chemistry AB, Hamnvägen 2, SE-444 85 Stenungsund, Sweden.

∥CR Competence AB, Center for Chemistry and Chemical Engineering, Lund University, P.O. Box 124, SE-221 00 Lund, Sweden.

Notes

The authors declare no competing financial interest.

■ ACKNOWLEDGMENTS

Sadly, Gerd Olofsson passed away on June 9, 2014. This article is dedicated to the memory of Gerd, a wonderful colleague and friend. K.S. and L.P. gratefully acknowledge the Swedish Research Council (VR) for individual grants, the Linnaeus grant Organizing Molecular Matter (239-2009-6749) through VR, and The Knut and Alice Wallenberg Foundation for a general instrument support to the Division of Physical Chemistry. We are grateful to Otto Glatter for letting us use his SAXS instrument at University of Graz, Austria, and to Petr Štěpánek, Institute of Macromolecular Chemistry, Prague, Czech Republic, for generously providing us with the REPES program. Luciano Galantini, Olle Söderman, and Daniel Topgaard are kindly acknowledged for fruitful discussions. Anette Mårtensson is thanked for help with some of the DLS measurements. M.T. acknowledges the financial support of the Slovenian Research Agency through the Physical Chemistry Program Group P1-0201.

■ REFERENCES

(1) Bronich, T. K.; Nehls, A.; Eisenberg, A.; Kabanov, V. A.; Kabanov, A. V. Novel Drug Delivery Systems Based on the Complexes of Block Ionomers and Surfactants of Opposite Charge. *Colloids Surf., B* **1999**, *16*, 243−251.

(2) Dubin, P. L.; Davis, D. D. Quasi-Elastic Light Scattering of Polyelectrolyte Micelle Complexes. *Macromolecules* **1984**, *17*, 1294−1296.

(3) Dubin, P. L.; Oteri, R. Turbidimetric Investigation of Mixed Micelle - Polyelectrolyte Interactions. In *Abstracts of Papers of the American Chemical Society*; American Chemical Society: Washington, DC, 1982; Vol. *183*, 122-POLY.

(4) Dubin, P. L.; Oteri, R. Association of Polyelectrolytes with Oppositely Charged Mixed Micelles. *J. Colloid Interface Sci.* **1983**, *95*, 453−461.

(5) Goddard, E. D. Polymer Surfactant Interaction. 2. Polymer and Surfactant of Opposite Charge. *Colloids Surf.* **1986**, *19*, 301−329.

(6) Hansson, P.; Lindman, B. Surfactant-Polymer Interactions. *Curr. Opin. Colloid Interface Sci.* **1996**, *1*, 604−613.

(7) Kamimura, M.; Kim, J. O.; Kabanov, A. V.; Bronich, T. K.; Nagasaki, Y. Block Ionomer Complexes of PEG-*block*-Poly(4-Vinylbenzylphosphonate) and Cationic Surfactants as Highly Stable. pH Responsive Drug Delivery System. *J. Controlled Release* **2012**, *160*, 486−494.

(8) Kwak, J. C. T. *Polymer-Surfactant Systems*; Marcel Dekker: New York, 1998; Vol. *77*.

(9) Ilekti, P.; Martin, T.; Cabane, B.; Piculell, L. Effects of Polyelectrolytes on the Structures and Interactions of Surfactant Aggregates. *J. Phys. Chem. B* **1999**, *103*, 9831−9840.

(10) Ilekti, P.; Piculell, L.; Tournilhac, F.; Cabane, B. How to Concentrate an Aqueous Polyelectrolyte/Surfactant Mixture by Adding Water. *J. Phys. Chem. B* **1998**, *102*, 344−351.

(11) Svensson, A.; Piculell, L.; Cabane, B.; Ilekti, P. A New Approach to the Phase Behavior of Oppositely Charged Polymers and Surfactants. *J. Phys. Chem. B* **2002**, *106*, 1013−1018.

(12) Hansson, P. Phase Behavior of Aqueous Polyion-Surfactant Ion Complex Salts: A Theoretical Analysis. *J. Colloid Interface Sci.* **2009**, *332*, 183−193.

(13) Hansson, P.; Almgren, M. Interaction of Alkyltrimethylammonium Surfactants with Polyacrylate and Poly(Styrenesulfonate) in Aqueous Solution: Phase Behavior and Surfactant Aggregation Numbers. *Langmuir* **1994**, *10*, 2115−2124.

(14) Almgren, M.; Hansson, P.; Mukhtar, E.; van Stam, J. Aggregation of Alkyltrimethylammonium Surfactants in Aqueous Poly(Styrenesulfonate) Solutions. *Langmuir* **1992**, *8*, 2405−2412.

(15) Kogej, K. Association and Structure Formation in Oppositely Charged Polyelectrolyte-Surfactant Mixtures. *Adv. Colloid Interface Sci.* **2010**, *158*, 68−83.

(16) Hansson, P. Self-Assembly of Ionic Surfactants in Polyelectrolyte Solutions: A Model for Mixtures of Opposite Charge. *Langmuir* **2001**, *17*, 4167−4180.

(17) Bronich, T. K.; Kabanov, A. V.; Kabanov, V. A.; Yu, K.; Eisenberg, A. Soluble Complexes from Poly(Ethylene Oxide)-*block*-Polymethacrylate Anions and N-Alkylpyridinium Cations. *Macromolecules* **1997**, *30*, 3519−3525.

(18) Herve, P.; Destarac, M.; Berret, J. F.; Lal, J.; Oberdisse, J.; Grillo, I. Novel Core-Shell Structure for Colloids Made of Neutral/Polyelectrolyte Diblock Copolymers and Oppositely Charged Surfactants. *Europhys. Lett.* **2002**, *58*, 912−918.

(19) Nisha, C. K.; Basak, P.; Manorama, S. V.; Maiti, S.; Jayachandran, K. N. Water-Soluble Complexes from Random Copolymer and Oppositely Charged Surfactant. 1. Complexes of Poly(Ethylene Glycol)-Based Cationic Random Copolymer and Sodium Dodecyl Sulfate. *Langmuir* **2003**, *19*, 2947−2955.

(20) Percebom, A. M.; Piculell, L.; Loh, W. Polyion-Surfactant Ion Complex Salts Formed by a Random Anionic Copolyacid at Different Molar Ratios of Cationic Surfactant: Phase Behavior with Water and n-Alcohols. *J. Phys. Chem. B* **2012**, *116*, 2376−2384.

(21) Pispas, S. Self-Assembled Nanostructures in Mixed Anionic-Neutral Double Hydrophilic Block Copolymer/Cationic Vesicle-Forming Surfactant Solutions. *Soft Matter* **2011**, *7*, 474−482.

(22) Berret, J. F.; Vigolo, B.; Eng, R.; Herve, P.; Grillo, I.; Yang, L. Electrostatic Self-Assembly of Oppositely Charged Copolymers and Surfactants: A Light, Neutron, and X-ray Scattering Study. *Macromolecules* **2004**, *37*, 4922−4930.

(23) Cohen Stuart, M. A.; Besseling, N. A. M.; Fokkink, R. G. Formation of Micelles with Complex Coacervate Cores. *Langmuir* **1998**, *14*, 6846−6849.

(24) Vitorazi, L.; Berret, J. F.; Loh, W. Self-Assembly of Complex Salts of Cationic Surfactants and Anionic Neutral Block Copolymers. Dispersions with Liquid Crystalline Internal Structure. *Langmuir* **2013**, *29*, 14024−14033.

(25) Dubin, P. L.; Elayne, M.; Vea, Y.; Fallon, M. A.; The, S. S.; Rigsbee, D. R.; Gan, L. M. Higher-Order Association in Polyelectrolyte Micelle Complexes. *Langmuir* **1990**, *6*, 1422−1427.

(26) Dubin, P. L.; Rigsbee, D. R.; McQuigg, D. W. Turbidimetric and Dynamic Light Scattering Studies of Mixtures of Cationic Polymers and Anionic Mixed Micelles. *J. Colloid Interface Sci.* **1985**, *105*, 509−515.

(27) Dubin, P. L.; The, S. S.; McQuigg, D. W.; Chew, C. H.; Gan, L. M. Binding of Polyelectrolytes to Oppositely Charged Ionic Micelles at Critical Micelle Surface-Charge Densities. *Langmuir* **1989**, *5*, 89−95.

(28) Thalberg, K.; Lindman, B.; Karlström, G. Phase Behavior of a System of Cationic Surfactant and Anionic Polyelectrolyte: The Effect of Salt. *J. Phys. Chem.* **1991**, *95*, 6004−6011.

(29) Svensson, A.; Norrman, J.; Piculell, L. Phase Behavior of Polyion-Surfactant Ion Complex Salts: Effects of Surfactant Chain Length and Polyion Length. *J. Phys. Chem. B* **2006**, *110*, 10332−10340.

(30) Piculell, L. Understanding and Exploiting the Phase Behavior of Mixtures of Oppositely Charged Polymers and Surfactants in Water. *Langmuir* **2013**, *29*, 10313−10329.

(31) Janiak, J.; Piculell, L.; Olofsson, G.; Schillen, K. The Aqueous Phase Behavior of Polyion-Surfactant Ion Complex Salts Mixed with Nonionic Surfactants. *Phys. Chem. Chem. Phys.* **2011**, *13*, 3126−3138.

(32) Janiak, J.; Bayati, S.; Galantini, L.; Pavel, N. V.; Schillén, K. Nanoparticles with Bicontinuous Cubic Internal Structure Formed by Cationic and Nonionic Surfactants and an Anionic Polyelectrolyte. *Langmuir* **2012**, *28*, 16536−16545.

(33) Nydén, M.; Söderman, O. Structures and Emulsification Failure in the Microemulsion Phase in the Didodecyldimethylammonium Sulfate/Hydrocarbon/Water System. A Self-Diffusion NMR Study. *Langmuir* **1995**, *11*, 1537−1545.

(34) da Silva, R. C.; Olofsson, G.; Schillén, K.; Loh, W. Influence of Ionic Surfactants on the Aggregation of Poly(Ethylene Oxide)-Poly(Propylene Oxide)-Poly(Ethylene Oxide) Block Copolymers

Studied by Differential Scanning and Isothermal Titration Calorimetry. *J. Phys. Chem. B* **2002**, *106*, 1239−1246.
(35) Jakob, C.; Schwarzbacher, A. T.; Hoppe, B.; Peters, R. A FPGA Optimised Digital Real-Time Mutichannel Correlator Architecture. In *10th Euromicro Conference on Digital System Design Architectures, Methods and Tools, Proceedings*; Kubatova, H., Ed.; IEEE Computer Society: Washington, DC, 2007; pp 35−42.
(36) Jakeman, E.; Pike, E. R. Spectrum of Clipped Photon Counting Fluctuations of Gaussian Light. *J. Phys. A* **1969**, *2*, 412−413.
(37) Berne, B. J.; Pecora, R. *Dynamic Light Scattering: With Applications to Chemistry, Biology And Physics*, 2nd ed.; Dover Publications, Inc: New York, 2000.
(38) Chu, B. *Laser Light Scattering: Basic Principles and Practice*, 2nd ed.; Academic Press: San Diego, 1991.
(39) Štěpanék, P. Data Analysis in Dynamic Light Scattering. In *Dynamic Light Scattering: The Method and Some Applications*; Brown, W., Ed.; Oxford University Press: Oxford, 1993; pp 177−240.
(40) Jakes, J. Regularized Positive Exponential Sum (REPES) Program—A Way of Inverting Laplace Transform Data Obtained by Dynamic Light Scattering. *Collect. Czech. Chem. Commun.* **1995**, *60*, 1781−1797.
(41) Schillén, K.; Jansson, J.; Löf, D.; Costa, T. Mixed Micelles of a PEO-PPO-PEO Triblock Copolymer (P123) and a Nonionic Surfactant ($C_{12}EO_6$) in Water. A Dynamic and Static Light Scattering Study. *J. Phys. Chem. B* **2008**, *112*, 5551−5562.
(42) Vink, H. J. Mutual Diffusion and Self-Diffusion in the Frictional Formalism of Non-Equilibrium Thermodynamics. *J. Chem. Soc., Faraday Trans. 1* **1985**, *81*, 1725.
(43) Brown, W.; Nicolai, T. Dynamic Properties of Polymer Solutions. In *Dynamic Light Scattering: The Method and Some Applications*; Brown, W., Ed.; Oxford University Press: Oxford, 1993; pp 272−318.
(44) Price, W. S. Pulsed-Field Gradient Nuclear Magnetic Resonance as a Tool for Studying Translational Diffusion. 1. Basic Theory. *Concepts Magn. Reson.* **1997**, *9*, 299−336.
(45) Stilbs, P. Fourier Transform Pulsed-Gradient Spin-Echo Studies of Molecular Diffusion. *Prog. Nucl. Magn. Reson. Spectrosc.* **1987**, *19*, 1−45.
(46) Bergmann, A.; Orthaber, D.; Scherf, G.; Glatter, O. Improvement of SAXS Measurements on Kratky Slit Systems by Gobel Mirrors and Imaging-Plate Detectors. *J. Appl. Crystallogr.* **2000**, *33*, 869−875.
(47) Orthaber, D.; Bergmann, A.; Glatter, O. SAXS Experiments on Absolute Scale with Kratky Systems using Water as a Secondary Standard. *J. Appl. Crystallogr.* **2000**, *33*, 218−225.
(48) Glatter, O. Data Treatment. In *Small Angle X-ray Scattering*; Glatter, O., Kratky, O., Eds.; Academic Press Inc. London Ltd.: London, 1983; 119−165.
(49) Fritz, G.; Glatter, O. Structure and Interaction in Dense Colloidal Systems: Evaluation of Scattering Data by The Generalized Indirect Fourier Transformation Method. *J. Phys.: Condens. Matter* **2006**, *18*, S2403−S2419.
(50) Weyerich, B.; Brunner-Popela, J.; Glatter, O. Small Angle Scattering of Interacting Particles. II. Generalized Indirect Fourier Transformation under Consideration of the Effective Structure Factor for Polydisperse Systems. *J. Appl. Crystallogr.* **1999**, *32*, 197−209.
(51) Lindner, P.; Zemb, T. *Neutrons, X-rays and Light: Scattering Methods Applied to Soft Condensed Matter*, 1st ed.; Elsevier: 2002.
(52) Glatter, O. Interpretation of Real-Space Information from Small Angle Scattering Experiments. *J. Appl. Crystallogr.* **1979**, *12*, 166−175.
(53) Fritz, G.; Bergmann, A.; Glatter, O. Evaluation of Small Angle Scattering Data of Charged Particles using the Generalized Indirect Fourier Transformation Technique. *J. Chem. Phys.* **2000**, *113*, 9733−9740.
(54) Brunner-Popela, J.; Mittelbach, R.; Strey, R.; Schubert, K. V.; Kaler, E. W.; Glatter, O. Small Angle Scattering of Interacting Particles. III. D_2O-$C_{12}E_5$ Mixtures and Microemulsions with n-Octane. *J. Chem. Phys.* **1999**, *110*, 10623−10632.
(55) Glatter, O. Data Evaluation in Small Angle Scattering—Calculation of Radial Electron-Density Distribution by Means of Indirect Fourier Transformation. *Acta Phys. Austriaca* **1977**, *47*, 83−102.
(56) Glatter, O. New Method for Evaluation of Small Angle Scattering Data. *J. Appl. Crystallogr.* **1977**, *10*, 415−421.
(57) Glatter, O. Evaluation of Small Angle Scattering Data from Lamellar and Cylindrical Particles by the Indirect Transformation Method. *J. Appl. Crystallogr.* **1980**, *13*, 577−584.
(58) Holmberg, K., Jönsson, B., Kronberg, B., Lindman, B. *Surfactants and Polymers in Aqueous Solution*, 2nd ed.; John Wiley & Sons: 2007.
(59) Jonströmer, M.; Jönsson, B.; Lindman, B. Self-Diffusion in Nonionic Surfactant Water-Systems. *J. Phys. Chem.* **1991**, *95*, 3293−3300.
(60) Brown, W.; Pu, Z.; Rymdén, R. Size And Shape of Nonionic Amphiphile Micelles: NMR Self-Diffusion and Static and Quasi-Elastic Light Scattering Measurements on $C_{12}E_5$, $C_{12}E_7$, and $C_{12}E_8$ in Aqueous Solution. *J. Phys. Chem.* **1988**, *92*, 6086−6094.
(61) Corti, M.; Minero, C.; Degiorgio, V. Cloud Point Transition in Nonionic Micellar Solutions. *J. Phys. Chem.* **1984**, *88*, 309−317.
(62) Imai, M.; Yoshida, I.; Iwaki, T.; Nakaya, K. Static and Dynamic Structures of Spherical Nonionic Surfactant Micelles During the Disorder-Order Transition. *J. Chem. Phys.* **2005**, *122*, 044906-1−044906-9.
(63) Kato, T.; Anzai, S.; Takano, S.; Seimuya, T. Intermicellar Interactions and Micelle Size Distribution in Aqueous Solutions of Polyoxyethylene Surfactants. *J. Chem. Soc., Faraday Trans. 1* **1989**, *85*, 2499−2509.
(64) Nilsson, P.-G.; Wennerström, H.; Lindman, B. Structure of Micellar Solutions of Nonionic Surfactants. Nuclear Magnetic Resonance Self-Diffusion and Proton Relaxation Studies of Poly-(Ethylene Oxide) Alkyl Ethers. *J. Phys. Chem.* **1983**, *87*, 1377−1385.
(65) Janiak, J.; Piculell, L.; Schillén, K.; Lundberg, D. Responsive Release of Polyanions from Soluble Aggregates Formed with a Hydrolyzable Cationic Surfactant and a Nonionic Surfactant. *Soft Matter* **2013**, *9*, 4103−4112.
(66) Hansson, P.; Schneider, S.; Lindman, B. Phase Separation in Polyelectrolyte Gels Interacting with Surfactants of Opposite Charge. *J. Phys. Chem. B* **2002**, *106*, 9777−9793.
(67) O. Söderman, personal communication.
(68) Nishikido, N. Solubilization in Mixed Micelles. In *Solubilization in Surfactant Aggregates*; Christian, S. D., Scamehorn, J. F., Eds.; Surfactant Science Series; Marcel Dekker: New York, 1995; Vol. *55*, pp 143−189.
(69) Le Maire, M.; Champeil, P.; Möller, J. V. Interaction of Membrane Proteins and Lipids with Solubilizing Detergents. *Biochim. Biophys. Acta* **2000**, *1508*, 86−111.
(70) Löf, D.; Tomsic, M.; Glatter, O.; Fritz-Popovski, G.; Schillén, K. Structural Characterization of Nonionic Mixed Micelles Formed by $C_{12}EO_6$ Surfactant and P123 Triblock Copolymer. *J. Phys. Chem. B* **2009**, *113*, 5478−5486.